Received: 23 October 2018 | Revised: 12 January 2019 | Accepted: 28 January 2019

DOI: 10.1002/ese3.295

RESEARCH ARTICLE

Energy Science & Engineering Open Access

Sputtering as a viable route for In_2S_3 buffer layer deposition in high efficiency $Cu(In,Ga)Se_2$ solar cells

Purvesh Soni[1] | **Mohit Raghuwanshi**[1] | **Roland Wuerz**[2] | **Birger Berghoff**[3] | **Joachim Knoch**[3] | **Dierk Raabe**[4] | **Oana Cojocaru-Mirédin**[1]

[1]RWTH Aachen, I. Physikalisches Institut (1A), Aachen, Germany

[2]Zentrum für Sonnenenergie- und Wasserstoff-Forschung Baden-Württemberg (ZSW), Stuttgart, Germany

[3]Institut für Halbleitertechnik, RWTH Aachen, Aachen, Germany

[4]Max-Planck-Institut für Eisenforschung GmbH, Düsseldorf, Germany

Correspondence
Purvesh Soni, RWTH Aachen, I. Physikalisches Institut (1A), Aachen, Germany.
Email: soni@physik.rwth-aachen.de

Funding information
Federal Ministry of Education and Research in Germany, NanoMatFutur BMBF project number 03X5522A.

Abstract

Alternative buffer layers in CIGSe are deposited mainly using chemical bath deposition because of its benefits like simplicity, good film quality and surface/step coverage. All the layers in CIGSe cell stack such as back contact, absorber and window layers are deposited by vacuum–deposition methods such as coevaporation, sputtering, and sometimes thermal evaporation, except for the buffer layer. Therefore, in the present work we demonstrate the feasibility to deposit In_2S_3 by RF magnetron sputtering reaching cell efficiencies of 13.6%, which is the highest value available for sputtered In_2S_3 in literature to date. Absorber surface damage and nonuniform buffer layer thickness are the primary limitations when using sputtering, and hence need to be eliminated for reaching reasonable cell efficiencies. We studied the extent of sputter induced damage on CIGSe absorber as well as the sputtering– and annealing–induced intermixing phenomenon at the In_2S_3/$Cu(In,Ga)Se_2$ interface at the subnanometer level using atom probe tomography. We have also shown that a post deposition annealing not only significantly improves the crystallinity of In_2S_3, but also recovers the surface damage caused by sputter-induced intermixing resulting in an improved p-n Junction quality (as shown by the electron beam induced current investigations), and substantially improves cell efficiency. The present work opens a new way for designing efficient and industry–compatible CIGSe cells using sputter–deposited Cd-free buffer layers. Moreover, this work clearly demonstrates that this novel and fully vacuum–deposited CIGSe cell meets the standard requirements, in terms of chemistry, structure, and electrical performance of a working cell for the PV industry.

1 | INTRODUCTION

Chalcopyrite thin–film solar cells containing chemically deposited CdS buffer layers have shown a record efficiency of 22.9%,[1] however its environmental concerns have motivated the PV community to look for a suitable replacement.

In_2S_3 is one substitute to the toxic CdS because of its better opto–electronic properties. The band gap of In_2S_3 ranges from 2.1 to 3.25 eV,[2-4] with direct or indirect band-to-band transitions. It has been observed that the bandgap of In_2S_3 varies with the employed deposition technique and the S/In stoichiometric ratio. A detailed study on the nature of band-to-band transition in In_2S_3 has been performed by Sterner et al.[5] In a recent study by Karthikeyan et al,[6] a direct bandgap of 2.77 eV has been obtained for sputtered In_2S_3 which is higher than that of CdS (2.4 eV).[7] Higher direct band gap

of the buffer layer is desirable since it gives better optical transmission at shorter wavelengths High cell efficiency is achieved by depositing In_2S_3 using thermal evaporation (PVD) with record efficiency of 18.2%[8] for 0.5 cm^2 cell. Industrial application of thermally evaporated In_2S_3 buffer layer is also very successful and has reached efficiency as high as 17.9%[9] for 30 × 30 cm^2 module which is comparable to the module efficiency of commercially available CIGSe solar cells with CdS buffer layer.[10]

It has been widely accepted in the photovoltaic community that sputtering can be a viable deposition method to chemical bath deposition (CBD) if it can produce large-scale, stable and high–efficiency devices.[11,12] Sputtering can be easily connected to the existing 3-stage coevaporation process used for the deposition of $Cu(In,Ga)Se_2$ (CIGSe) absorber obtaining thus an end-to-end dry vacuum based industrial production line.[13] For CBD-CdS buffer layers, the CIGSe absorber are removed from the vacuum for deposition and reintroduced in the vacuum chamber for ZnO–sputter deposition. On the contrary, sputtered In_2S_3 buffer layer deposition can be extended to the existing ZnO deposition process. The main advantage of this process is higher throughput and better reproducibility of commercial CIGSe modules under clean conditions. Avoiding exposure to air ensures impurity free surfaces/interfaces which prevents the formation of deep defects in the band gap and shunting pathways, and thus minimizes unwanted recombination at interfaces.[14] These criterions are extremely important for achieving high–efficient cells.

There are a few drawbacks when depositing In_2S_3 by sputtering, which need to be considered. Sputtering of In_2S_3 directly on the CIGSe absorber may induce sputter damages to the CIGSe surface that results in a high density of defects in the region near the p-n junction. Moreover, poor film uniformity results when the buffer layers are sputter deposited on a ~100 nm rough CIGSe surface.[15] Therefore, in the present work, we will present viable strategies to prevent or at least to considerably decrease these two drawbacks by first applying supplementary heat-treatment of the In_2S_3 buffer at 210°C for 15 minutes and, second, by working with thicker In_2S_3 buffer layers (several tens of nanometers) to obtain a good surface and step coverage (contrary to the CBD deposition method where extremely thin layers of ~30 nm[16] can already give a very good surface and step coverage). In the present work, we will show that by limiting these two drawbacks, we could successfully reach 13.6% cell efficiency for the RF–sputtered In_2S_3 buffer layer, which is the highest cell efficiency among all reported studies in literature for In_2S_3 buffer layers deposited by sputtering.[17]

Moreover, in the present work we applied atom probe tomography (APT) technique,[18] which is contrary to any other existing experimental techniques such as Auger electron spectroscopy (AES),[19] secondary ion mass spectroscopy (SIMS),[20] and energy dispersive X-ray spectroscopy (EDX) is able to trace the elemental redistributions at the subnanometer level without being influenced by the CIGSe surface roughness. Based on these APT investigations, the sputtering– and annealing–induced intermixing phenomenon between the In_2S_3 buffer layer and the CIGSe absorber is studied here. These compositional results at the In_2S_3/CIGSe heterointerface are finally directly correlated to the electrical properties of the p-n junction of the device using electron beam induced current (EBIC) investigations.

2 | EXPERIMENTAL SECTION

2.1 | Sample preparation

In_2S_3 buffer layers were deposited on a 25 × 25 mm CIGSe/Mo–coated soda lime glass substrate in a single step using rf magnetron sputtering. The sputter unit was custom designed with three cathodes in a confocal configuration by Aurion GmbH, Germany. To remove any undesired oxides, the surface of the CIGSe absorbers was cleaned[11] in 10% NH_4OH solution for 5 minutes, rinsed in DI water and dried with nitrogen gas prior to In_2S_3 sputtering. The substrates were transferred immediately into the load lock chamber of the sputter tool under high vacuum of ~10^{-7} mbar to avoid oxidation and/or contamination of the cleaned CIGSe surface. These samples were kept for drying in the load lock chamber for about 30 minutes before transferring them to the sputter chamber for the In_2S_3 deposition. In_2S_3 thin films were then sputtered on the CIGSe absorbers at room temperature using a 4" diameter stoichiometric In_2S_3 target. The sputtering was performed under high purity argon (6N) gas and under a working pressure of ~3×10^{-3} mbar and background pressure of ~10^{-8} mbar. The target to substrate distance was fixed at 50 mm with a sputtering power of 1.27 W/cm^2 and a substrate rotation speed of 10 RPM. For this work, the CIGSe absorbers were obtained from Zentrum für Sonnenenergie- und Wasserstoff-Forschung (ZSW) GmbH, Stuttgart, Germany. The CIGSe layers (about 2.1 μm thick) were grown in a multi–stage inline coevaporation process on Mo–coated soda lime glass substrate at about 600°C.[21] The 0.55 μm thick Mo was deposited on the soda lime glass substrate using dc magnetron sputtering.[22]

On top of the In_2S_3 buffer layer, intrinsic ZnO and ZnO:Al were deposited with the same sputter setup using the secondary and tertiary cathodes of the sputter unit. i-ZnO was sputtered at 3×10^{-3} mbar sputter pressure and at 2.5 W/cm^2 sputter power while ZnO:Al (AZO) was sputtered at 5×10^{-3} mbar sputter pressure and at 3.2 W/cm^2 sputter power. Metal contacts of Ni/Al with a thickness of ~10 nm/1.5 μm, respectively were deposited by e-beam evaporation using a shadow mask. The sample was then

annealed in air at 210°C for 15 minutes and mechanically scribed into eight cells of 0.5 cm^2 each. The obtained CIGSe cells with ~85 nm-thick In_2S_3 buffer layer before heat treatment are named hereafter as In_2S_3 -RT (85 nm) and after air annealing at 210°C for 15 minutes are named as In_2S_3 -HT (85 nm). Likewise, samples with a 25 nm In_2S_3 buffer layer after a similar air annealing step will be called In_2S_3 -HT (25 nm).

2.2 | Optimization of the sputtering deposition of In_2S_3 buffer layer

During sputtering, a significant difference between the vapor pressures of In and S (1 mBar at 1200°C for In v/s 1 mBar at 175°C for S) may induce a nonstoichiometric composition for the deposited In_2S_3 thin-film. Although the In_2S_3 composition is influenced by both, the sputter power and working pressure, the strongest influence on the In_2S_3 composition is exercised by the sputter power as shown in Table 1. It is worthwhile to note here that higher sputter powers (≥1.91 W/cm^2) gave good and consistent In/S ratios but resulted in nonuniform films with an inferior step coverage, whereas lower sputter power (≤0.63 W/cm^2) gave good conformal films but slow sputtering rates and inconsistent In/S stoichiometric ratios. The value of 1.27 W/cm^2 was chosen as a reliable compromise between film uniformity and In_2S_3 stoichiometry. Too high sputter power notably increases the sputtering–induced intermixing, a scenario which should be avoided to achieve a defect–free In_2S_3/CIGSe heterojunction. An optical transmission of 70-80% was obtained for films with a thickness ~80 nm deposited at 1.27 W/cm^2 which changes only a little when changing the pressure (see Figure S1). A stable plasma was obtained at 3×10^{-3} mbar and thus this pressure was chosen for deposition of In_2S_3 buffer layers.

The linear dependence between the thickness of the deposited In_2S_3 film and sputtering time was determined using scanning transmission electron microscopy (STEM) in high angle annular dark–field imaging (HAADF) mode, as we had recently shown in Ref.[23] At 1.27 W/cm^2 power and 3×10^{-3} mbar working pressure (which were also used as the primary deposition parameters for this work), the average film thickness after 5 minutes of sputtering was found to be on average ~ 85 nm, although the film thickness was found to vary between ~30 to ~110 nm as clearly seen in Figure 1. The difference in thickness is due to the very rough topography of the CIGSe absorber causing a shadowing effect for the sputtered atoms arriving at the substrate surface which makes the buffer film thinner in valleys and at steps and thicker at peaks and flat-top surfaces. One way to overcome this issue is to sputter at very slow rates and increase the substrate rotation speed for a conformal coverage with uniform buffer layer thickness.

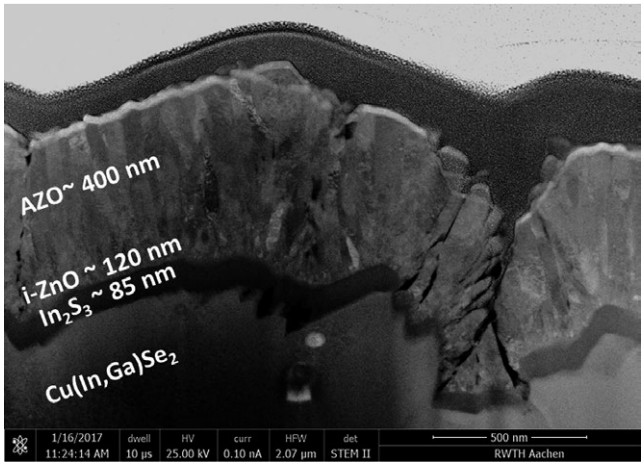

FIGURE 1 STEM HAADF image of the cross section of a In_2S_3 -HT (85 nm) sample showing the multilayer structure, that is AZO/i-ZnO/In_2S_3/CIGSe. The buffer layer deposition is thicker on peaks or flat CIGS topography whereas thinner in valleys and steps. Cracks in window layers may form shunting paths which is detrimental for the device performance

Thinner buffer layers are very desirable for their enhanced transmission behavior in the blue wavelength region of the electromagnetic spectrum (see Results section) but are not very reliable in long term service since it is very difficult to obtain a uniform surface coverage on CIGSe by sputtering. For this work, besides an 85 nm In_2S_3 buffer layer, we also deposited 25 nm In_2S_3 buffer layers for comparison. Some of the devices with 25 nm-thick In_2S_3 layer showed 11.2% efficiency (see Table 2), but the achieved average cell efficiency was only ~6% characterized by a low average fill factor.

The crystallinity of the sputter–deposited In_2S_3 buffer layer was investigated by high–resolution TEM (HRTEM). Figure 2 shows the HRTEM image of the i-ZnO/In_2S_3/CIGSe stack. First, the HRTEM studies show that the In_2S_3 layer was amorphous right after deposition as proven by X-ray diffraction investigations (not shown here), whereas it became nanocrystalline (with an approximate crystallite size of about 10 nm as seen in Figure 2B) after annealing. Moreover, the selected area electron diffraction (SAED) pattern in Figure 2C shows a mixture of spot and ring patterns, which clearly states that the In_2S_3 buffer layer was not fully crystallized after an annealing at 210°C for 15 minutes. Second, the

TABLE 1 Energy dispersive X-ray composition of In and S measured for different sputter powers and pressures

Sputter power (W/cm^2)	Sputter pressure (mbar)	In (at. %)	S (at. %)
0.63	3×10^{-3}	41.9 ± 1.0%	58.1 ± 1.0%
1.27	3×10^{-3}	40.5 ± 1.0%	59.5 ± 1.0%
1.91	3×10^{-3}	42.5 ± 1.0%	57.5 ± 1.0%

TABLE 2 The measured values of the efficiency (ɳ), open circuit voltage (V_{OC}), short–circuit current density (J_{SC}), and fill factor (FF) are given for the CdS-reference and In_2S_3 sputtered buffer layer samples. Significant improvement in device parameters was observed after annealing

Sample	ɳ (%)	V_{OC} (mV)	J_{SC} (mA/cm^2)	FF (%)
CdS – Reference	16.1	673	31.95	75
In_2S_3 – RT (85 nm)	0.9	143	20.71	36
In_2S_3 – HT (85 nm)	13.6	688	32.52	53
In_2S_3 – HT (25 nm)	11.2	503	26.54	51

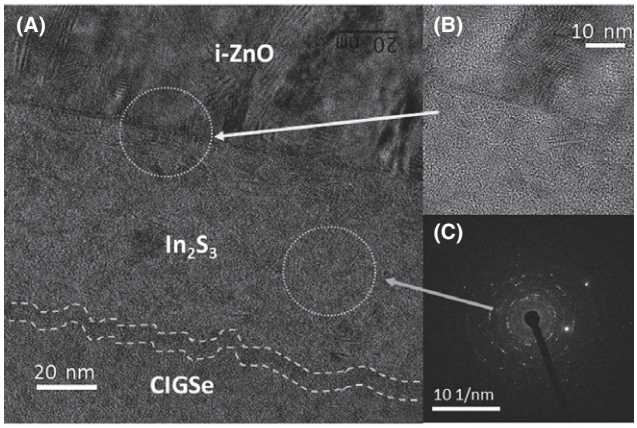

FIGURE 2 HRTEM image of In_2S_3-HT (85 nm) sample showing (A) the i-ZnO/In_2S_3/CIGSe stack (B) nanocrystalline structure of In_2S_3 and i-ZnO layers and (C) SAED pattern of the buffer layer, the CIGSe/In_2S_3 interface is marked as a dashed line

HRTEM studies showed clearly neither the presence of secondary phases such as Cu_2Se and Ga_2O_3 or In_2O_3 nor the presence of ordered defects compounds (ODC) at the CIGSe surface as suggested by Cojocaru-Mirédin et al[23] and Abou-Ras et al.[24]

2.3 | Characterization methods

To determine the composition of sputtered films, 500 nm-thick In_2S_3 film were deposited on Si (110) substrates. The elemental composition of pure–In_2S_3 films was measured using EDX installed on FEI Helios Nanolab 650 microscope using Oxford Instruments X-Max 80 mm^2 SDD-EDS detector at 20 kV acceleration voltage and 0.4 nA electron beam current. The acceleration voltage and beam current used for the EDX studies were optimized on a stoichiometric In_2S_3 sputter target. At 20 kV acceleration voltage and 0.4 nA beam current, the In:S ratio showed the best match to their respective atomic ratio with an error around ±1%. This error is empirically determined by measuring the composition of the stoichiometric In_2S_3 target.

The structure and thickness of the buffer and window layers were measured using STEM in HAADF mode in the same FEI microscope at 25 kV and 0.1 nA. HRTEM investigations were performed on a JEOL 2200 fs TEM operating at 200 kV. EQE measurements were performed using a spectral quantum efficiency measurement tool IQE-Scan manufactured by PV-tools GmbH, Germany. Cell efficiency and I-V measurements were performed using an Oriel solar simulator Sol3A Class AAA at 100 W/cm^2 equipped with Keithley 2400 source meter with AM 1.5 standard spectrum from Newport corporation, USA.

Atom probe tomography measurements were performed using a LEAP 4000X Si from Cameca Instruments, USA. Probing was conducted in laser mode by applying UV–laser pulses of 355 nm wavelength at 40 K, 12 ps pulse length, 5 pJ laser pulse energy and a repetition rate of 250 kHz. Needle shaped APT samples were prepared from CIGSe devices containing the In_2S_3/CIGSe interface within the first 100 nm of the apex of the needle–shaped specimen. APT specimens were prepared by using the standard lift out method described in Ref.[25] To minimize/remove beam damage and amorphous surface layer of the APT-sample, a low energy (5 keV) Ga beam was used at the final ion–milling stage. The obtained needle–shaped samples containing the In_2S_3/CIGSe interface were transferred immediately to the APT chamber to avoid any surface contamination on them. To perform the STEM/HRTEM investigations, a lamella of dimensions 20 × 5×2 µm was cut from the CIGSe device and mounted on a Mo–TEM grid by platinum welding. The lamella was thinned down to a thickness of approximatively 50 nm so that it is transparent enough to the incident electrons of energy varying from 30 to 200 kV.

Electron beam induced current measurements were performed at room temperature using Gatan Smart EBIC integrated in a FEI Helios nanolab 650 microscope at 20 kV and 0.2 nA. The cross section was cut in FIB using Ga–ion beam with an acceleration voltage of 16 kV and a beam current of 0.79 nA. This was done to reduce artifacts arising due to electron accumulation on uneven surfaces. The low–kV cleaning (at 5 kV and 0.16 nA) step was then used to minimize the surface amorphization.

3 | RESULTS

3.1 | Device characterizations

External quantum efficiency (EQE) measurements were performed on samples In_2S_3-HT (25 nm) and In_2S_3-HT (85 nm) as shown in Figure 3. These experiments show that the cells containing a thinner In_2S_3 buffer, that is 25 nm, had a better charge carrier collection probability in the blue energy region between 300 and 500 nm, whereas those containing a thicker In_2S_3 buffer, that is 85 nm, had better charge collection in the visible region between 600 and 1000 nm. This can be due

to higher overall Na–doping concentration in thinner In_2S_3 which results in a wider bandgap[26] at the same annealing temperature as compared to thicker In_2S_3 buffer layer. There was also a small difference in the red response of the two spectra, which is possibly due to minor changes in absorber properties from sample to sample.

The measured I-V characteristics of the cells investigated in this work are shown in Table 2. The In_2S_3 – RT (85 nm) sample show poor open circuit voltage (V_{OC}) of 193 mV and a low fill factor (FF) of 36%. After annealing at 210°C for 15 minutes, a significant improvement in efficiency from 0.9% to 13.6% and in V_{OC} from 193 mV to 688 mV was observed. For the In_2S_3 – HT (25 nm) sample a much lower V_{OC} and short circuit current (J_{SC}) value was recorded with a small difference in FF as compared to the 85 nm In_2S_3 device. The diode ideality factor calculated from the ln(J) – V curve was found to be as high as 6.62, which was probably due to the low shunting resistance of 71.02 Ω.cm^2 recorded for the best performing cell with efficiency 13.6%. A similar annealing treatment is also required for CBD and thermally evaporated buffer layers to suppress the interfacial recombination due to presence of defect states formed at the hetero-interface. However, for sputtered buffer layers, annealing treatment also cures the sputter–induced damages to CIGSe absorber surface at the hetero-interface.

3.2 | Elemental distribution at the nanoscale using atom probe tomography

Atom probe tomography experiments were performed on In_2S_3 – RT (85 nm) and In_2S_3 – HT (85 nm) samples to understand how sputtering of the In_2S_3 buffer layer affects the local elemental distribution at the CIGSe surface within the first few nanometers.

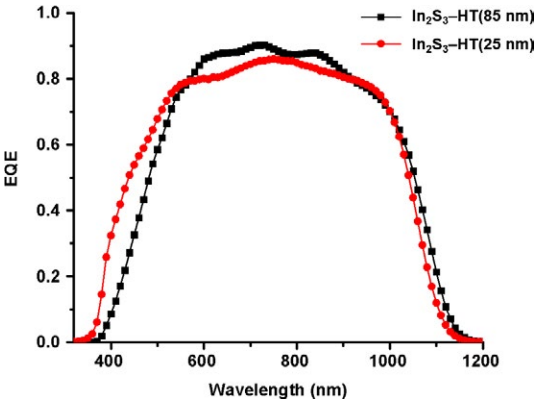

FIGURE 3 External quantum efficiency (EQE) curves of sputtered In_2S_3 buffer layer with a thickness of 25 nm (-●-) and 85 nm (-■-) after annealing at 210°C for 15 min. The thinner (25 nm) buffer layer shows a better response in the UV region of the spectrum. When calculating J_{sc} from the EQE curves one gets similar J_{SC} values (30.7 mA/cm^2 for 85 nm and 27.6 mA/cm^2 for 25 nm)

Figure 4A,B shows the three dimensional elemental distribution at the Cu(In,Ga)Se_2/In_2S_3 interface for In_2S_3 – RT (85 nm) and In_2S_3 – HT (85 nm) samples, whereas Figure 4C,D shows their respective proximity histogram (or proxigram; for more information refer to ref.[27]). These proxigrams are divided into three regions: (I) Cu–depleted CIGSe surface (so-called CIGSe surface reconstruction[28]), (II) interfacial intermixing region and (III) heat induced intermixing region.

Region I of the In_2S_3 – RT (85 nm) sample was artificially modified mainly by the high energetic In atoms (In is heavier than Cu, Ga, and Se) inducing a sputter damaged region with a size larger than 3 nm (see Figure 4C). In region I, the Cu-depletion was accompanied by an In-enrichment, showing thus an In–Cu anticorrelation.[29] After annealing (see Figure 4D), the region I of In_2S_3 – HT (85 nm) sample showed an even stronger depletion in Cu and enrichment in In. In contrast, APT experiments performed on a chemically deposited In_2S_3 buffer layer[23] showed a Cu–depleted CIGS surface of approximatively 3 nm but almost no change in In concentration.

Region II in Figure 4C was assigned to the *interfacial intermixing* between In_2S_3 and CIGSe. It is believed that the sputter–induced intermixing zone in this case is maximum ~2.5 nm. We note here, that the 2 nm width of the intermixed region measured from the proxigram is the improved value obtained after applying very gentle deposition conditions. Interface intermixing of similar magnitude (1-2 nm) has been previously observed for chemically deposited CdS or In_2S_3 buffers.[23,30] This suggests that the sputter damages were considerably reduced when depositing In_2S_3 buffers with the previously mentioned sputter parameters. In this work, after annealing (see Figure 4D), the width of the intermixed region became wider by approximatively 3.5 nm. This is mainly due to the heat–induced intermixing or diffusion of mainly Cu towards the In_2S_3 layer and In, S towards the CIGSe layer. Especially for Cu, a continuous diffusion profile starting from CIGSe and continuing inside In_2S_3 in region III is observed as shown in Figure 4D. Region III in Figure 4D is thus entirely assigned to the heat–induced intermixing between In_2S_3 and CIGSe.

However, such a heat–induced intermixed region is also observed for the nonannealed sample, that is for In_2S_3 – RT (85 nm) sample. It is known that during sputtering, besides the sputtering–induced intermixing process, a considerable amount of heat is generated locally by the bombardment of energetic sputtered atoms. The maximum temperature measured directly on the CIGSe absorber using a point contact thermocouple during sputtering was 75°C, however the actual temperature on the surface can be much higher. This promotes elements to slightly diffuse during the sputter deposition process, explaining thus the existence of a small region III of ~1 nm-thick for the In_2S_3 – RT (85 nm) sample. In this small region, only Cu was found to diffuse proving thus the high mobility of Cu.

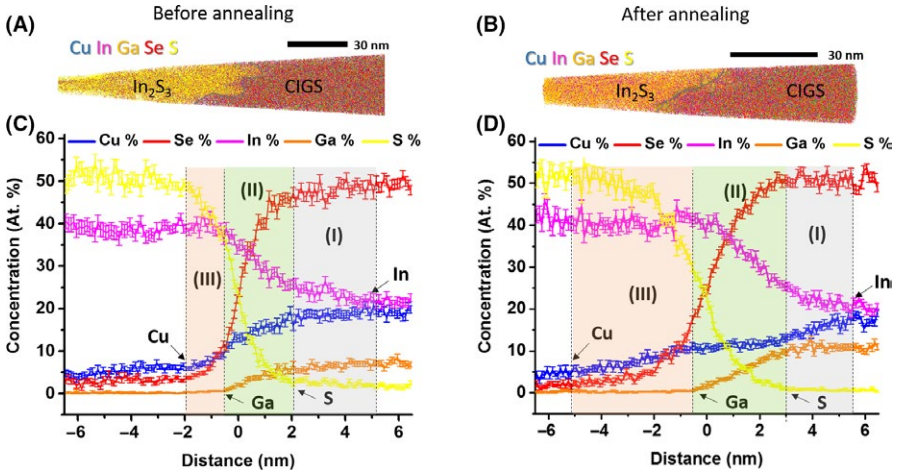

FIGURE 4 3D elemental map of In_2S_3/CIGSe interface for (A) In_2S_3 – RT (85 nm) and (B) In_2S_3 – HT (85 nm) samples showing the redistribution of Cu (blue), In (pink), Ga (orange), Se (red) and S (yellow). (C and D) exhibit the proximity histograms in the region of the In_2S_3/CIGSe hetero-interface. There is redistribution of all elements after the heat treatment, but the Cu concentration profile is significantly flattened after annealing. This has made the CIGSe surface Cu-deficient, moreover, S and In are diffusing into the CIGSe surface

TABLE 3 The measured concentration of In (indium), S (sulfur), Cu (copper), Ga (gallium), Se (selenium), H(hydrogen) and O (oxygen) for In_2S_3 and CIGSe layers within the first 50 nanometers from the interface before and after annealing. A significant drop in S concentration is seen after annealing due to its low vapor pressure, change in In_2S_3 crystallinity and elemental redistribution across the interface

Layer	Sample	In	S	Cu	Ga	Se	H	O
In_2S_3	In_2S_3 – RT (85 nm)	38.06 ± 0.16%	56.35 ± 0.01%	2.65 ± 0.04%	0.01 ± 0.00%	1.83 ± 0.02%	0.65 ± 0.01%	0.45 ± 0.01%
	In_2S_3 – HT (85 nm)	49.60 ± 0.14%	47.12 ± 0.02%	1.67 ± 0.04%	—	1.60 ± 0.02%	—	—
CIGS	In_2S_3 – RT (85 nm)	18.37 ± 0.07%	—	20.34 ± 0.06%	9.64 ± 0.05%	50.36 ± 0.03%	0.92 ± 0.01%	0.35 ± 0.01%
	In_2S_3 – HT (85 nm)	18.25 ± 0.09%	—	22.12 ± 0.07%	9.66 ± 0.06%	49.97 ± 0.03%	—	—

An estimation of the In and S concentrations by the proxigram is not precise due to the peak overlaps ($^{65}S_2^+$ with $^{65}Cu^+$ and $^{97}S_3^+$ with $^{97}CuS^+$) observed in the mass-to-charge spectrum. To overcome this limitation, the mass spectra of the In_2S_3 layer and the CIGSe layer in the proximity of the junction were evaluated separately and precise elemental concentrations were obtained by decomposing the convoluted peaks in accordance to the ratio of their isotopic abundance. The obtained values for both layers, before and after annealing are shown in Table 3. A significant loss of S in the In_2S_3 layer from 56.35 at.% to 47.12 at.% was found after annealing. This led to a significant change in the In_2S_3 stoichiometric ratio as shown in Table 3.

Our experiments show that Cu was found to diffuse from the CIGSe into the In_2S_3 buffer layer at temperatures above 210°C and thus further depleting Cu from the CIGSe surface. Figure 5 compares the proximity histogram of Cu for both samples, that is In_2S_3 – RT (85 nm) and In_2S_3 – HT (85 nm). For sample In_2S_3 – RT (85 nm) the Cu drop is abrupt at the interface. However, after annealing, there is a significant depletion of Cu on the CIGSe side making the surface region overall Cu-poor. This change in Cu composition significantly modifies the local doping at the interface region. By further annealing the sample In_2S_3 – HT (85 nm) for 45 minutes at 210°C, even more pronounced Cu diffusion into the In_2S_3 layer (making the CIGSe surface even more Cu-deficient) is observed.

3.3 | EBIC investigations

Electron beam induced current analysis was used to investigate the charge carrier activity in the device before and after annealing. Figure 6(A-D) shows the SEM image and the corresponding EBIC map obtained for In_2S_3 – RT (85 nm) and In_2S_3 – HT (85 nm) samples. Here bright contrast represents increased minority charge carrier (here electrons) collection or current collection and vice versa. The space charge region (SCR) emerges brightest due to maximum separation of charge carriers which occur in this region. We note here that the space charge region is approximately 500 nm deep into CIGSe extending from the buffer layer. Moreover, the J-EBIC (junction-EBIC) image

shows that most of the grains in the CIGSe bulk are active and contribute to the EBIC current, which was consistent over several cross sections studied for this device. This indicates that the buffer and window layers are uniformly deposited on the absorber. Figure 6E shows the EBIC/Ebeam line profile obtained from the regions marked in the EBIC images. The position 0 where the EBIC current peaks are located represents the position of the electrical junction which clearly coincides with the physical junction present at the buffer–absorber interface. It is evident from Figure 6E that the overall EBIC current has significantly increased after annealing.

4 | DISCUSSIONS

4.1 | Opto–electronic properties

Before annealing, the cells showed very low V_{OC} values implying a very defective p-n junction. This is attributed to the fact that the CIGSe surface is damaged by the highly energetic In and S atoms during In_2S_3 deposition, creating a high density of interfacial defects. Using SRIM calculations,[31] the average kinetic energy of In and S atoms was calculated based on the penetration depths given by APT data of 4 and 1.5 nm, respectively. The calculated values for the averaged kinetic energy are ~0.7 and 0.2 keV, respectively. Moreover, the EBIC experiments clearly showed a considerably decreased current collection before annealing. This is explained by the presence of a high number of radiative and SRH recombination active defects at the CIGSe surface which can adversely affect the cell efficiency.

After annealing, the significant increase in V_{OC} value, and hence in cell efficiency, clearly indicates the improved p-n junction quality. The latter one can be explained by (a) the passivation of interfacial defects, (b) improved crystallinity of In_2S_3 buffer, and (c) diffusion of Cu across the interface. However, it is believed that the V_{OC} and hence efficiency values can be further improved by completely crystallizing the In_2S_3 layer. The presence of a small fraction of amorphous In_2S_3 indicates that the In_2S_3/CIGSe interface may still contain recombination active centers. Moreover, the low fill factor value of 53%, low shunting resistance of 71.02 Ω.cm^2, high ideality factor of 6.62 and a nonlinear ln(J) – V behavior indicates that there is still room for improvement of the device quality.

The J_{SC} values varies only little after annealing as seen in Table 2. Based on Ref.[32] the J_{SC} is directly proportional to the diffusion length of minority carriers, that is to the diffusion length of the electrons (l_e) or holes (l_h) for In_2S_3, such as $J_{SC} = eG(I_e + w + I_h)$, where G is the generation rate and w is the width of the depletion region. The fact that J_{SC} had not changed upon annealing (no modification of l_e or l_h) means that no deep defects had been introduced in CIGS and In_2S_3 bulk during sputtering, that is no considerable recombination phenomenon takes place in the CIGSe or In_2S_3 bulk. This observation proves that the V_{OC} is the most affected parameter by sputtering of the In_2S_3 buffer layer, that is sputtering drastically increases the recombination phenomenon at the interface region.

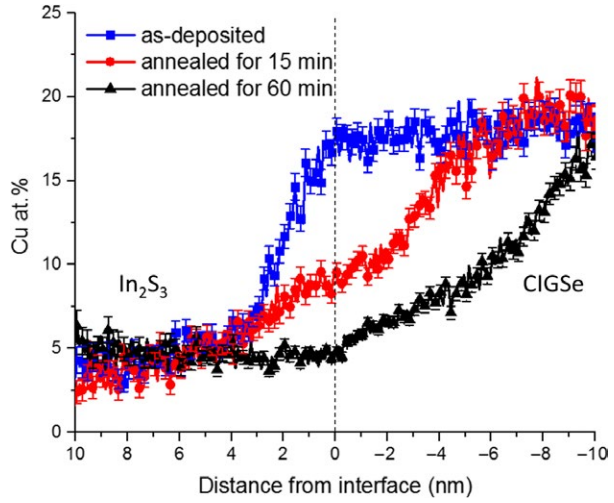

FIGURE 5 Cu proximity histogram close to the interface for the In_2S_3 – RT (85 nm) sample before annealing (blue), after 15 min annealing at 210°C (In_2S_3 – HT (85 nm) sample (red) and 60 min annealing (black). These concentration profiles show how Cu diffusion into the In_2S_3 layer depletes Cu from the CIGSe surface on prolonging the annealing time at 210°C

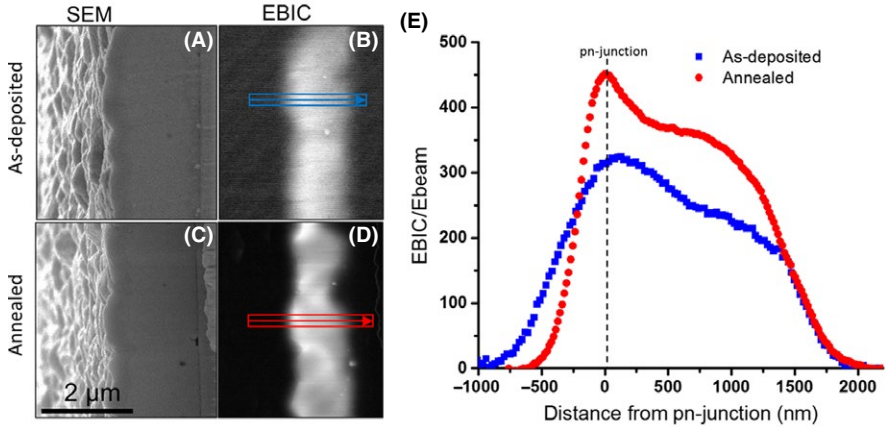

FIGURE 6 A-D are the SEM images and the corresponding EBIC maps of AZO/i-ZnO/In_2S_3/CIGS/Mo stack before and after annealing at 210°C. E, EBIC/Ebeam depth profiles for the respective samples obtained from the indicated regions in the EBIC maps. The dotted line in (E) represents the position of the p-n junction. These depth profiles show the improved current collection at the p-n junction for the sample annealed at 210°C for 15 min

The EBIC results demonstrate formation of a uniform continuous p-n junction across the CIGSe layer which is crucial for solar cell operation. The enhancement in the overall intensity of J-EBIC spectra after annealing indicates a better charge carrier separation at the p-n junction, that is the interface between the buffer and the absorber layers (Figure 6A-D). A better carrier separation leads to a better collection of carriers resulting in an overall increase in efficiency of the device. Hence, EBIC results agree well with the increased efficiency observed for annealed samples. In addition, we can also see a narrowing of the peak at the p-n junction which is a good indicator of the improvement in the junction quality, crystallinity of In_2S_3, and passivation of interfacial defects.

4.2 | Compositional analysis

The APT results support the opto–electronic properties, that is the enhanced Cu–depletion behavior at the CIGSe surface after annealing impacts positively the cell efficiency. We suggest that the Cu vacancies (V_{Cu}^{-}) are occupied by In antisites (In_{Cu}^{2+}) in this region. The latter ones act as donor defects leading to a downward band bending and, hence, Fermi level pinning at the interface close to the conduction band. This effect improves the total charge carrier concentration in CIGS and, hence, the V_{OC} value.

Moreover, the interfacial intermixing region (II) in Figure 4 had also completely changed after annealing. We mainly observed a partial passivation/substitution of Se by S. The selenium vacancies (V_{Se}) in CIGSe are donor–like defects that promote n-type conductivity in CIGSe which are detrimental to the cell efficiency, are replaced by sulphur. Sulfur also passivates these vacancies and dangling bonds near the CIGSe surface[33] thus sulfurizing the absorber surface. This results in an enhanced bandgap of CIGSe which improves the band alignment with In_2S_3 resulting in a higher charge carrier concentration of the p-n junction.[34] A similar process happens when Cu vacancies are passivated by Sulfur at the CIGSe surface. This inter-diffusion and surface passivation on annealing largely suppresses the interfacial defects. Bär et al[35] studied the intermixing at the In_2S_3/CIGSe interface and found that a pronounced inter-diffusion at the In_2S_3/CIGSe interface improves the band alignment. This lowers the e-h recombination and enhances the photosensitivity of the device. Thus the combined process of Fermi–level pinning in region I and sulfurization/defect passivation of region II significantly increases the absorber bandgap locally and minimizes undesired interfacial recombination by suppressing the electrical charge defects.[35] This may be a plausible reason for the substantial improvement in V_{OC} observed after annealing.

As already mentioned before, we were able to determine experimentally that Cu diffuses into the In_2S_3 layer not only after annealing but also before annealing that is during sputter deposition at room temperature. It should however be noted that before annealing, to identify if any clustering of Cu has taken place, the maximum separation method[18] was used. The first nearest neighbor distance (1NN) was calculated in the region close to the interface. The obtained data distribution overlapped with the randomized reference data (see Figure S4) suggesting that there is no cluster formation for Cu in In_2S_3.

The heat induced intermixing region (III) is formed by the diffusion of Cu across the junction interface before and after annealing. From Figure 5, we can see that after annealing, a significant amount of Cu has diffused into the In_2S_3 layer making the interface region overall Cu-deficient. This trend continues by further annealing the sample for 45 minutes.

Cu diffusion in In_2S_3 bulk might have a significant effect on the solar cell performance. Pronounced Cu diffusion into the In_2S_3 bulk is detrimental since it lowers the In_2S_3 bandgap blocking the blue region of the solar spectrum due to formation of complex Cu-In-S based ternary alloys.[36] This can occur when the Cu-concentration in In_2S_3 reaches an upper solubility limit of about 10%.[37,38] This means that a lower amount of Cu diffusing into the In_2S_3 is beneficial since it not only improves In_2S_3 crystallinity by passivating the In vacancies, but also makes the interface region Cu-deficient without forming Cu-In-S phases. In this work, the maximum Cu-concentration found in In_2S_3 for the highest cell efficiency of 13.6% was 4.0 at.%. Although not concise, the Cu-content in the In_2S_3 layer obtained in this work seems to be a good compromise between In_2S_3 defect passivation and avoiding formation of Cu-In-S phases in the In_2S_3 buffer layer.

It has been inferred from several studies[39,40] that Cu diffusion in In_2S_3 layers above 200°C improves the In_2S_3 crystallinity. In this work, we have found that annealing at 210°C for 15 minutes only partially crystallizes the amorphous In_2S_3. Even with a partly crystalline In_2S_3 buffer layer, we were successful in achieving a high efficiency CIGSe device.

Interestingly, a higher Cu concentration of 2.65 ± 0.04 at.% was detected by APT in In_2S_3 for the nonannealed In_2S_3 – RT (85 nm) than for the annealed In_2S_3 – HT (85 nm) sample which was 1.67 ± 0.04 at.%. This is not unusual since out of the several samples analyzed by APT after annealing, the copper concentration found in the In_2S_3 ranged from 1.5 at.% to up to 4 at.%. Nonconsistency in Cu concentration mainly depends on the interface geometry which is directed by the CIGSe topography. As evident from the HAADF images, the CIGSe topography has unevenly distributed valleys and peaks. In_2S_3 is comparatively thinner in the valleys as compared to the peaks because of the shadowing effect during sputter deposition. Thus, In_2S_3 deposited in the valleys will have a higher overall concentration of copper in its vicinity as compared to In_2S_3 deposited at the peaks. On the other hand, the volume fraction of In_2S_3 is lower in valleys owing to its lower thickness. This means that the amount of Cu in In_2S_3 may vary depending on the local surface geometry of CIGSe as presented in Figure 7. This can also change the crystallinity of In_2S_3 locally.

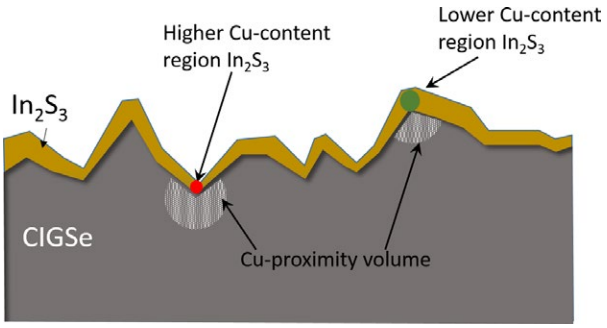

FIGURE 7 Variation of local Cu concentration with respect to In_2S_3 buffer layer thickness. Thinner buffer layer deposited in the valleys have much higher Cu content in its proximity than the thicker In_2S_3 deposited at the peaks which results in nonuniform Cu-diffusion in the buffer layer

After annealing, no traces of Na were found in the bulk and interface region of CIGSe and In_2S_3 layers, however a small amount (0.2 at.%) Na was found segregated at the In_2S_3/CIGSe interface for another region of the same sample (see Figure S3). The presence of Na close to the CIGSe surface has been previously reported by our group[41,42] suggesting the diffusion of Na from grain boundaries to the buffer/absorber interface. The present work agrees with the work from our group which suggests that the presence of Na at the interface does not depend on the annealing temperature but rather on the vicinity of the interface to a Na–rich CIGS grain boundary.

5 | SUMMARY

We produced relatively high–efficiency CIGSe devices using sputtered In_2S_3 buffer layers with a scope of further improvement. The compositional and opto–electronic properties of the high efficiency samples were studied mainly using APT, EBIC and EQE. We were able to map the elemental interdiffusion profile at the In_2S_3/Cu(In,Ga)Se_2 interface in the nanoscale regime by using atom probe tomography before and after annealing. We could also determine the extent of the absorber surface damage incurred by the In_2S_3 buffer layer deposition. However, the absorber surface damaged by sputtered atoms was restored by annealing, which not only improved In_2S_3 crystallinity, but also significantly enhanced the V_{OC}. EBIC measurements supported these findings which showed significant enhancement of charge carrier collection of the device after annealing. From the EBIC measurements, we also found that the physical and electrical junction in In_2S_3/CIGSe solar cells overlap. We have clearly shown the effect of annealing on elemental diffusion across the interface. The Cu-poor surface of CIGSe is significantly enlarged after annealing by prominent diffusion of Cu into the In_2S_3. Likewise, S passivation of the CIGSe surface on annealing also may play a major role in improving the device performance. Moreover, we found that the amount of Cu diffusing into the In_2S_3 may be dependent on the local surface geometry of the absorber–buffer interface. Hence the present work highlights that In_2S_3 is a promising alternative buffer layer material and is ideal for sputter deposition. The electrical and chemical nanoscale characterization provides novel routes for improving further the efficiency.

ACKNOWLEDGMENTS

This work is funded by the Federal Ministry of Education and Research in Germany within the Atomsonde Project (NanoMatFutur BMBF project 03X5522A), which is gratefully acknowledged.

ORCID

Purvesh Soni https://orcid.org/0000-0001-5551-8948
Mohit Raghuwanshi https://orcid.org/0000-0003-4352-072X
Birger Berghoff https://orcid.org/0000-0003-3567-8121

REFERENCES

1. Kamada R, Yagioka T, Adachi S, et al. New world record Cu(In, Ga)(Se, S)2 thin film solar cell efficiency beyond 22%. 2016 IEEE 43rd Photovoltaic Specialists Conference (PVSC). 2016:5.
2. Barreau N, Bernède JC, Marsillac S. Study of the new β-In2S3 containing Na thin films. Part II: optical and electrical characterization of thin films. *J Cryst Growth*. 2002;241(1):51-56.
3. Asikainen T, Ritala M, Leskelä M. Growth of In2S3 thin films by atomic layer epitaxy. *Appl Surf Sci*. 1994;82-83:122-125.
4. Yousfi EB, Asikainen T, Pietu V, Cowache P, Powalla M, Lincot D. Cadmium-free buffer layers deposited by atomic later epitaxy for copper indium diselenide solar cells. *Thin Solid Films*. 2000;361(Supplement C):183-186.
5. Sterner J, Malmström J, Stolt L. Study on ALD In2S3/Cu(In, Ga)Se2 interface formation. *Prog Photovoltaics Res Appl*. 2005;13(3):179-193.
6. Karthikeyan S, Hill AE, Pilkington RD. Low temperature pulsed direct current magnetron sputtering technique for single phase β-In 2 S 3 buffer layers for solar cell applications. *Appl Surf Sci*. 2017;418:199-206.
7. Ernits K, Brémaud D, Buecheler S, et al. Characterisation of ultrasonically sprayed InxSy buffer layers for Cu(In, Ga)Se2 solar cells. *Thin Solid Films*. 2007;515(15):6051-6054.
8. Spiering S, Nowitzki A, Kessler F, Igalson M, Abdel Maksoud H. Optimization of buffer-window layer system for CIGS thin film devices with indium sulphide buffer by in-line evaporation. *Sol Energy Mater Sol Cells*. 2016;144:544-550.
9. Module with record efficiency from AVANCIS: Fraunhofer ISE certifies CIGS solar module with an efficiency of 17.9%. 2016.
10. Yang S. Achievement of 16.5% total area efficiency on 1.09 m^2 CIGS modules in TSMC solar production line. 2015 IEEE 42nd Photovoltaic Specialist Conference (PVSC), New Orleans, LA. 2015:1-3.
11. Klenk R, Steigert A, Rissom T, et al. Junction formation by Zn(O, S) sputtering yields CIGSe-based cells with efficiencies exceeding 18%. *Prog Photovoltaics Res Appl*. 2014;22(2):161-165.

12. Grimm A, Kieven D, Lauermann I, et al. Zn(O, S) layers for chalcopyrite solar cells sputtered from a single target. *EPJ Photovolt*. 2012;3:30302.
13. Powalla M, Witte W, Jackson P, et al. CIGS cells and modules with high efficiency on glass and flexible substrates. *IEEE J Photovolt*. 2014;4(1):440-446.
14. Liao Y-K, Kuo S-Y, Hsieh M-Y, et al. A look into the origin of shunt leakage current of Cu(In, Ga)Se2 solar cells via experimental and simulation methods. *Sol Energy Mater Sol Cells*. 2013;117:145-151.
15. Kodigala SR. Chapter 3 – Surface analyses of I-III–VI2 compounds. In: Subba Ramaiah K, ed. *Thin Films and Nanostructures*. Cambridge, MA: Academic Press; 2010:55-113.
16. Alexander JN, Higashiya S, Caskey D, Efstathiadis H, Haldar P. Deposition and characterization of cadmium sulfide (CdS) by chemical bath deposition using an alternative chemistry cadmium precursor. *Sol Energy Mater Sol Cells*. 2014;125:47-53.
17. Hariskos D, Menner R, Lotter E, Spiering S, Powalla M. Magnetron sputtering of indium sulphide as the buffer layer in Cu(InGa)Se2-based solar cells. 20th European Photovoltaic Solar Energy Conference, 6-10 June 2005, Barcelona, Spain, 2005: 4.
18. Miller MK. *Atom Probe Tomography*. New York, NY: Springer; 2000.
19. Huang C, Li SS, Shafarman W, et al. Study of Cd-free buffer layers using Inx(OH, S)y on CIGS solar cells. *Sol Energy Mater Sol Cells*. 2001;69(2):131-137.
20. Eicke A, Spiering S, Dresel A, Powalla M. Chemical characterisation of evaporated In2Sx buffer layers in Cu(In, Ga)Se2 thin-film solar cells with SNMS and SIMS. *Surf Interface Anal*. 2008;40(3–4):830-833.
21. Wuerz R, Eicke A, Kessler F, Paetel S, Efimenko S, Schlegel C. CIGS thin-film solar cells and modules on enamelled steel substrates. *Sol Energy Mater Sol Cells*. 2012;100:132-137.
22. Zhou D, Zhu H, Liang X, et al. Sputtered molybdenum thin films and the application in CIGS solar cells. *Appl Surf Sci*. 2016;362:202-209.
23. Cojocaru-Mirédin O, Fu Y, Kostka A, et al. Interface engineering and characterization at the atomic-scale of pure and mixed ion layer gas reaction buffer layers in chalcopyrite thin-film solar cells. *Prog Photovoltaics Res Appl*. 2015;23(6):705-716.
24. Abou-Ras D, Kostorz G, Strohm A, Schock H-W, Tiwari A. Interfacial layer formations between Cu(In, Ga)Se[sub 2] and In[sub x]S[sub y] layers. *J Appl Phys*. 2005;98(12):123512.
25. Blum I, Cuvilly F, Lefebvre-Ulrikson W. Atom probe sample preparation. In: Lefebvre W, Vurpillot F, Sauvage X, eds. *Atom Probe Tomography: Put Theory Into Practice*. Cambridge, MA: Academic press; 2016:97-121.
26. Barreau N, Bernède JC, Marsillac S, Amory C, Shafarman WN. New Cd-free buffer layer deposited by PVD: In_2S_3 containing Na compounds. *Thin Solid Films*. 2003;431–432:326-329.
27. Hellman OC, Vandenbroucke JA, Rüsing J, Isheim D, Seidman DN. Analysis of three-dimensional atom-probe data by the proximity histogram. *Microsc Microanal*. 2000;6(5):437-444.
28. Mönig H, Fischer C-H, Caballero R, et al. Surface Cu depletion of Cu(In, Ga)Se2 films: an investigation by hard X-ray photoelectron spectroscopy. *Acta Mater*. 2009;57(12):3645-3651.
29. Abou-Ras D, Schmidt SS, Caballero R, et al. Confined and chemically flexible grain boundaries in polycrystalline compound semiconductors. *Adv Energy Mater*. 2012;2(8):992-998.
30. Cojocaru-Mirédin O, Choi P, Wuerz R, Raabe D. Atomic-scale characterization of the CdS/CuInSe2 interface in thin-film solar cells. *Appl Phys Lett*. 2011;98(10):103504.
31. Ziegler JF, Ziegler MD, Biersack JP. SRIM – The stopping and range of ions in matter (2010). *Nucl Instrum Methods Phys Res, Sect B*. 2010;268(11-12):1818-1823.
32. Smets A, Zeman M, Isabella O, van Swaaij R. *Solar Energy: The Physics and Engineering of Photovoltaic Conversion, Technologies and Systems*. Cambridge: UIT Cambridge; 2016.
33. Nam Y, Yoo J, Chang SK, et al. Photoluminescence of sulfur-incorporated CIGS solar cells through post-annealing. *J Lumin*. 2017;188:595-599.
34. Chen S-H, Lin W-T, Chan S-H, et al. Photoluminescence analysis of CdS/CIGS interfaces in CIGS solar cells. *ECS J Solid State Sci Technol*. 2015;4(9):347-350.
35. Bär M, Barreau N, Couzinié-Devy F, et al. Impact of annealing-induced intermixing on the electronic level alignment at the In2S3/Cu(In, Ga)Se2 thin-film solar cell interface. *ACS Appl Mater Interfaces*. 2016;8(3):2120-2124.
36. Barreau N, Deudon C, Lafond A, Gall S, Kessler J. A study of bulk NaxCu1−xIn5S8 and its impact on the Cu(In, Ga)Se2/In2S3 interface of solar cells. *Sol Energy Mater Sol Cells*. 2006;90(12):1840-1848.
37. Pistor P, Abou Ras D, Lauermann I, Rissom T, Schmidt S, Klenk R. Cu diffusion and junction formation at the (PVD-) In2S3 buffer layer/Cu(In,Ga)Se2 absorber interface. 2010:2881-2884.
38. Zheng Z, Yu J, Cheng S, Lai Y, Zheng Q, Pan D. Investigation of structural, optical and electrical properties of Cu doped β-In2S3 thin films. *J Mater Sci: Mater Electron*. 2016;27(6):5810-5817.
39. Juma AO, Pistor P, Fengler S, Dittrich T, Wendler E. Copper diffusion in thin In2S3 layers investigated by Rutherford Backscattering Spectroscopy. *Thin Solid Films*. 2012;520(22):6740-6743.
40. Pistor P, Allsop N, Braun W, et al. Cu in In2S3: interdiffusion phenomena analysed by high kinetic energy X-ray photoelectron spectroscopy. *Phys Status Solidi (a)*. 2009;206(5):1059-1062.
41. Cojocaru-Mirédin O, Choi P, Wuerz R, Raabe D. Exploring the p-n junction region in Cu(In, Ga)Se2 thin-film solar cells at the nanometer-scale. *Appl Phys Lett*. 2012;101(18):181603.
42. Koprek A, Cojocaru-Miredin O, Wuerz R, Freysoldt C, Gault B, Raabe D. Cd and impurity redistribution at the CdS/CIGS interface after annealing of CIGS-based solar cells resolved by atom probe tomography. *IEEE J Photovolt*. 2017;7(1):313-321.

SUPPORTING INFORMATION

Additional supporting information may be found online in the Supporting Information section at the end of the article.

How to cite this article: Soni P, Raghuwanshi M, Wuerz R, et al. Sputtering as a viable route for In_2S_3 buffer layer deposition in high efficiency Cu(In,Ga)Se_2 solar cells. *Energy Sci Eng*. 2019;7:478-487. https://doi.org/10.1002/ese3.295